Computers and Electronics in Agriculture 215 (2023) 108464

Contents lists available at ScienceDirect

Computers and Electronics in Agriculture

journal homepage: www.elsevier.com/locate/compag

Filament-necking localization method via combining improved PSO with rotated rectangle algorithm for safflower-picking robots

Zhenyu Xing [a,c], Zhenguo Zhang [a,b,*], Ruimeng Shi [a], Quanfeng Guo [a], Chao Zeng [a]

[a] College of Mechanical and Electrical Engineering, Xinjiang Agricultural University, Urumqi 830052, China
[b] Key Laboratory of Xinjiang Intelligent Agricultural Equipment, Urumqi 830052, China
[c] Key Laboratory of Intelligent Equipment and Robotics for Agriculture of Zhejiang Province, Hangzhou 310058, China

ARTICLE INFO

Keywords:
Picking robots
Visual localization
Image segmentation
Improved PSO algorithm
Future farming

ABSTRACT

Safflower is one of the most important specialty economic crops in the world. Safflower blossoms are harvested continuously for 3–5 times. Untimely picking can affect the opening of filaments in the next crop, resulting in reduced filament production and serious economic losses. However, the safflower images collected by picking robots were affected by lighting conditions or complex backgrounds. The existing segmentation algorithms have the problem of insufficient segmentation or over-segmentation, because of the small safflower size and localization area. Therefore, combining improved particle swarm optimization (PSO) with a rotated rectangle algorithm based on the filament-necking localization method for safflower-picking robots was proposed. The R-component image in RGB color space was extracted as a preprocessing sample by combining the color features of safflower. The inertia weights in the PSO algorithm are improved to enhance the performance of the algorithm. An adaptive nonlinear function is introduced to search for the optimal threshold and initially segmented to obtain the binary image. Then, the barycenter and minimum outer rectangle of the contour were set up using the rotated rectangle algorithm based on the geometric features of the filaments. The circular region of interest (Cir-ROI) of filament-necking is determined. The Zhang-Suen refinement algorithm was used for skeleton extraction to design an algorithm for localizing the picking point of safflower filaments. To test safflower images collected in complex environments, the results of average processing time were 0.14 s, and the average relative target area error rate was 19.33 %. Moreover, the localization accuracy of the picking point was 89.75 %. The filament-necking localization method provides a theoretical basis and experimental data support for damage reduction and efficient harvesting of safflower filaments.

1. Introduction

The worldwide sown area of safflower was 122,000 ha in 2022(De Oliveira Neto et al., 2022; Zhang et al., 2023a). China is one of the major safflower producers in the world (Gongora et al., 2022; Zhang et al., 2023b). Since safflower bears multiple clusters of small, numerous, compact, and dense filaments, the filaments segmentation is key to the precise localization of picking point in robots picking (Campos et al., 2016; Abbood et al., 2020). Currently, the vision camera of safflower-picking robots is often used to observe safflower and machine vision is employed to perceive the growth of safflower and the change of the environments in real time (Dischinger et al., 2021; Qiao et al., 2023). However, the external optical variations and backgrounds in the images captured are considerably complex, such as clouds, branches and leaves, plant shadows, and other objects far away from the camera (Benbarrad et al., 2021). The color and texture feature information of the captured safflower become blurred in the edge and non-edge regions. Therefore, improving the efficiency and quality of picking safflower is important.

To reduce damage to safflower filaments by picking robots, keeping the intact filaments, and utilizing safflower images to further study the phenotype of safflower filaments, it is necessary to first segment the filaments from the images. Then, the optimal picking area was detected on the segmented filament image and accurately locates the picking point of safflower filaments in the picking area. This method can effectively avoid the loss of other filaments caused by the robotic picking process, which would affect the re-opening of the filaments, leading to reduced filament yield and quality (Singh et al., 2021a; Li et al., 2022). However, the quality of filament segmentation is often severely affected

* Corresponding author.
E-mail address: zhangzhenguo@xjau.edu.cn (Z. Zhang).

https://doi.org/10.1016/j.compag.2023.108464
Received 30 August 2023; Received in revised form 23 October 2023; Accepted 21 November 2023
Available online 1 December 2023

by factors such as noise, variations in light intensity, overall safflower scale, and crop shading in complex environments (Gao et al., 2023). By enhancing or decreasing the brightness and saturation of the image, the color and texture features of the safflower filaments become more distinguishable. Generalized image segmentation technology allowed for the segmentation of filament images, which is an important basis for image recognition and localization of picking points (Qiao et al., 2019). In addition, the color of the picking point for safflower filaments is similar to that of the leaf and crop shadows. Picking points were difficult to identify and locate accurately and output coordinates (Dischinger et al., 2021; Su et al., 2021). Nevertheless, machine vision can sense the growth condition of crops in real time, solving the phenomenon of feature blurring and difficult segmentation due to the complex environments of safflower filaments. Therefore, machine vision technology is used to position the picking point in real time and assist the intelligent safflower-picking robot in picking accurately.

Machine vision technology is characterized by non-contact and automation, providing a low-cost and efficient for real-time crop picking (Kumar et al., 2022; Soltani et al., 2022). The recognition and segmentation of fruits are one of the core technologies for automated picking in agricultural robots (Gongal et al., 2015b; Li et al., 2023a,b). To address the problem of accurate segmentation and recognition of crops, Yogesh et al. (2020) and Sabzi et al. (2019) segmented the pixels of the region using fruit size, contour, and texture features and extracted them. Behroozi-Khazaei and Maleki (2017) proposed a robust algorithm based on ANN and GA for segmenting grape clusters and leaves from the background using color features was developed. GA was employed for optimizing of ANN structure and selecting supreme color features simultaneously. Wang et al., (2019a) investigated a color-independent segmentation method. The method combines features of image saliency and contours to segment apple fruits from naturally illuminated, different-colored apple images. Zou et al. (2022) proposed a method for designing a color index based on different tasks. This method adapts to changes in the external environment. Fan et al. (2021) proposed a patch-based gray-centered color space segmentation algorithm. The algorithm can segment apples with bright and dark patches, keeping the geometry of the segmentation target. Li et al., (2017; 2018) recognized green apples under complex backgrounds combining the texture, shape, and color features of the image. The method provided better segmentation results for fruits with light background occlusion. Chithra and Henila (2021) proposed an algorithm for segmenting out ROI from apple fruit images. Segmentation of regions of interest in color images of apple fruits using GTA was performed with an accuracy of 96.67 %. Although the above method solved the problem of crop recognition and segmentation in terms of size, color, and texture features, it was only applicable to cases where there were significant differences (color, brightness, etc.) between the target to be segmented and the background.

Recently, scholars have also researched the localization and segmentation of crop-picking point. Xiong et al. (2017) obtained binary images of grape bunches through Ostu threshold segmentation in solving the visual localization problem of the picking point. At the same time, Hough straight line fitting was used to determine the picking point. Luo et al. (2015) obtained the ROI above the outer rectangle by image segmentation. Similarly, the position of the picking point on the fruit stalk was determined by screening the straight line with the closest distance to the barycenter. However, most of the studies about picking safflower are focused on mechanized positioning. Zhang et al. (2018) and Ge et al. (2015) proposed an improved morphological processing method for contour transformation to obtain the two-dimensional center point coordinates of the filaments by combining the improved picking point and the method of the maximum internal tangent circle. Chen et al. (2021) proposed the principle of set strip pre-positioning, which adjusted the distribution state of single safflower fruit balls from spatially disordered to strip-ordered, reducing the difficulty of recognizing and picking the safflower. In summary, the studies found that crop picking mainly focused on the recognition and segmentation of crops and the calculation of the geometric dimensions for crops. In contrast, the segmentation and localization algorithms need to be designed for the features of different targets (Montoya-Cavero et al., 2022; Bai et al., 2023). Vision camera for agricultural robots is unable to discriminate the color and texture features of safflower because of the influence of light variations, branches, leaves, plant shadows, and other objects in the edge and non-edge regions of the safflower. Further exploration is needed for safflower image segmentation.

The PSO algorithm is a globally optimized and locally convergent search algorithm that has been used in areas such as path planning, and automatic control. Pandey et al. (2010) proposed an algorithm for task scheduling problems based on PSO to minimize the cost and time. Ritu and Kumar (2014) proposed a multi-objective list scheduling algorithm to optimize the reliability and completion time of constraint vector partitioning for scientific workflow. The PSO algorithm had faster convergence than other heuristics and used fewer algorithm parameters than other heuristics, which made the algorithm less dependent on parameter tuning (Jatmiko et al., 2007). However, the PSO algorithm was prone to premature convergence. Therefore, to improve the recognition and localization accuracy of safflower-picking robots, the segmentation method of safflower filament images based on the improved PSO and rotated rectangle algorithm was proposed. Firstly, according to the color features of safflower, the maximum connectivity region of segmented filaments is extracted with the improved PSO algorithm. The inertia weights and adaptive nonlinear function in the PSO algorithm are improved to enhance the performance of the algorithm. Then, the re-segmentation method based on the geometric features of filaments is used to determine the circular ROI. Finally, using the Zhang-Suen refinement algorithm for skeleton extraction, the localization method of filaments is designed to enable efficient and low-loss intact safflower-picking. The main contributions of the proposed approach include:

(1) To effectively reduce the interference of the background region on safflower filament detection and strengthen the global and local search capability, the optimal threshold is searched by an improved PSO algorithm with safflower filament as the target feature. The redesigned fitness function dynamically adjusts the optimality-seeking global search for safflower to maximize the extraction of complete safflower filaments. Meanwhile, edge and non-edge local convergence of safflower is performed to make the population update the historical optimal fitness value and position and segment the safflower.

(2) The barycenter and contour minimum outer rectangle of safflower filaments was set up using the rotated rectangle algorithm based on the geometric features of the filaments, which determines the Cir-ROI of filament-necking. The algorithm effectively solves the problem of picking point localization errors caused by variations in light intensity and crop shadows.

(3) Combining the primary segmentation and re-segmentation results, the structure of safflower is analyzed. The backbone is extracted by the Zhang-Suen refinement algorithm. Meanwhile, the localization method of picking point is designed. The background noise mixed into the re-segmentation results is effectively suppressed.

The remainder of this study is organized as follows. Section 2 explains relevant materials; Section 3 describes the localization method in this research; Section 4 lists the experimental setup and evaluation indicators; Section 5 shows the experimental results and them; Section 6 makes a discussion; finally, Section 7 makes conclusions and lists future works.

2. Materials

2.1. Acquisition of image data

The opening safflower consists mainly of filaments, necks, and fruiting ball, characterized by wide filament spread and a large fruiting ball (Zhang et al., 2022). Filaments are either solitary or arranged in corymb-like inflorescences, and symmetrically distributed. Safflower

images were collected using an RGB-D camera on July 10–20, 2023 at the safflower planting base in Qapaqal Xibe Autonomous County, Yili, Xinjiang, China. The precise localization design of the safflower-picking robot is closely related to the physical features of the safflower in the opening period. The physical features of safflower are measured with the widely planted safflower "Jinhong 8″ as the studied object in the opening period. It can provide the design and theoretical basis for the optimization of robot positioning schemes and structures. The measurement results are shown in Table 1. The position and process of the safflower-picking robot were simulated during the shooting, as shown in Fig. 1.

The collected images contained different colors, postures, sizes, and light conditions sunny day with light, sunny day with backlight, overcast day with light, and cloudy day with light. According to the main material feature parameters of safflower in Table 1, the height of the camera from the ground was determined to be 700 mm. The angle with the vertical direction was 90°, with the horizontal distance from the safflower of 200 mm. The camera was facing a single safflower, collecting the image format as.jpg and the size of 1018 × 764 pixels. A total of 800 safflower images were collected, including 400 test images (100 images each of different weather conditions). Fig. 2 illustrates the samples for four different weather conditions. To improve the computational efficiency, the original image resolution was compressed to 1000 × 600 pixels before computation.

2.2. Characterization of safflower-picking point

The rectangular necking of the picking area connects filaments to the fruiting ball. In addition, the filament-necking area is composed of filaments and necking. To achieve a lower breakage rate of safflower filaments, the picking region needs to be sufficiently small and precise. The rectangular necking of the picking area includes the part of the necking and a few filaments at the connection site with it. The Cir-ROI of filament-necking is the rectangular necking of the picking area and a part of the filament-necking, as shown in Fig. 3. Center of the circle is located in the same longitudinal axis as the barycenter of the safflower filaments and fruit ball. Therefore, the accuracy of picking point localization increases when the Cir-ROI of filament-necking contains larger areas of the rectangular necking of the picking area. Meanwhile, the localized picking point can minimize the breakage rate of safflower filaments when the barycenter of the safflower filaments and fruit ball is located on the same longitudinal axis.

3. Methods

3.1. Method overview

The flow of the filament-necking localization method for safflower-picking robots is shown in Fig. 4. The method consists of three parts: (i) the primary segmentation model with an improved PSO algorithm based on color features; (ii) the re-segmentation model with rotated rectangle based on geometric features; (iii) and the localization of picking point model using the Zhang-Suen skeleton refinement algorithm.

During the localization of the picking point, the collected images of safflower were preprocessed. Firstly, the improved PSO algorithm based on color features was used for initial segmentation to extract the binary image of the maximum connectivity region of safflower filaments. Then, the rotated rectangle method based on the geometric features was used to solve the filaments barycenter and contour minimum outer rectangle. In turn, the segmentation extracted the Cir-ROI of filament-necking. Finally, the Zhang-Suen skeleton refinement algorithm was applied to the re-segmentation results to extract and design the localization of the picking point.

Table 1
Main material feature parameters of safflower in the opening period.

Parameter	Numerical value	Mean value
Filaments width /mm	30.44–59.35	50.33 ± 2.88
Necking diameter /mm	2.93–6.97	5.30 ± 0.78
Filaments height /mm	17.28–25.90	20.01 ± 2.30
Safflower plant height /mm	643.20–783.70	700.40 ± 5.85

3.2. Primary segmentation based on color features

3.2.1. Target extraction of R-component variability

The identification and localization of the picking point are key to separating the target of safflower filaments from the background (Rico-Fernández et al., 2019; Jiang et al., 2023). The background consists of surrounding safflower, foliage, branches, and other foreign objects. Since filaments are distinguishable in color from background features, color has been used as the basis for differentiation (Castillo-Martínez et al., 2020). Considering the complexity of light in the actual field environment, the factors may generate uneven lighting, shadows, and bright shifts, and excessive light, all of which can complicate color separation. Therefore, the filament-necking localization method adopted the RGB color model. This model was easy to implement in hardware and separated color and grayscale information.

With the safflower growing, the content of red pigment in filaments increased gradually. The color of safflower filaments keeps changing from yellow to red continuously, as shown in Fig. 5. According to the growth features of filaments during the opening period when the filaments were immature, they mainly showed yellow color, as shown in Fig. 5(a). It made the R gray value smaller than the G gray value in the safflower image (R-G < 0). When the filaments were half-ripe, they mainly consisted of orange and yellow, as shown in Fig. 5(b) and Fig. 5(c). There were some regions in the image of safflower filament where the R gray value was smaller than the G gray value. Instead, when the filaments were ripe, they were red, as shown in Fig. 5(d) and Fig. 5(e). It made the R grayscale value of the image significantly larger than the G grayscale value (R-G > 0). In addition, the safflower at the time of shedding was crimson, but not available for picking, as shown in Fig. 5(f). Therefore, through the extraction of RGB color components, the three components were combined in the operation. The results show that the histogram double-peak effect of the R component for filaments was more obvious in the opening period, as shown in Fig. 6(a)-(c). However, there was no significant double-peak phenomenon in R, G, and B of safflower filaments in the flower-shedding period, as shown in Fig. 6(d)-(f).

3.2.2. Improved PSO algorithm

The PSO algorithm seeks the global optimum by following the currently searched optimum. To emphasize the difference between the safflower filaments and other regions, the requirement of minimum segmentation error is satisfied in cases where the single-peak, multi-peak, or double-peak effect of the RGB color component histograms is not satisfactory (Xue et al., 2019; Singh et al., 2021b). Meanwhile, the localized coarse segmentation of safflower filaments is reduced and the localized convergence of the edges is improved. Therefore, the PSO algorithm (Jatmiko et al., 2007) allows each particle to be considered a pixel point. The position of each particle represents the region to which the pixel point belongs and the velocity represents the moving speed of the pixel point. PSO algorithm searches the global image of safflower and localized convergence of the edges of filaments. After continuous search and iteration, the safflower images are divided into safflower filaments and other different regions to improve the accuracy of filament segmentation.

An improved PSO algorithm is used to segment safflower images. The idea of the improved PSO algorithm is mainly to initialize the velocity and position of the particle swarm first. Then, the inertia weights are utilized to search for the current individual extreme value and global solution. Finally, the particle adaptation value is calculated and the

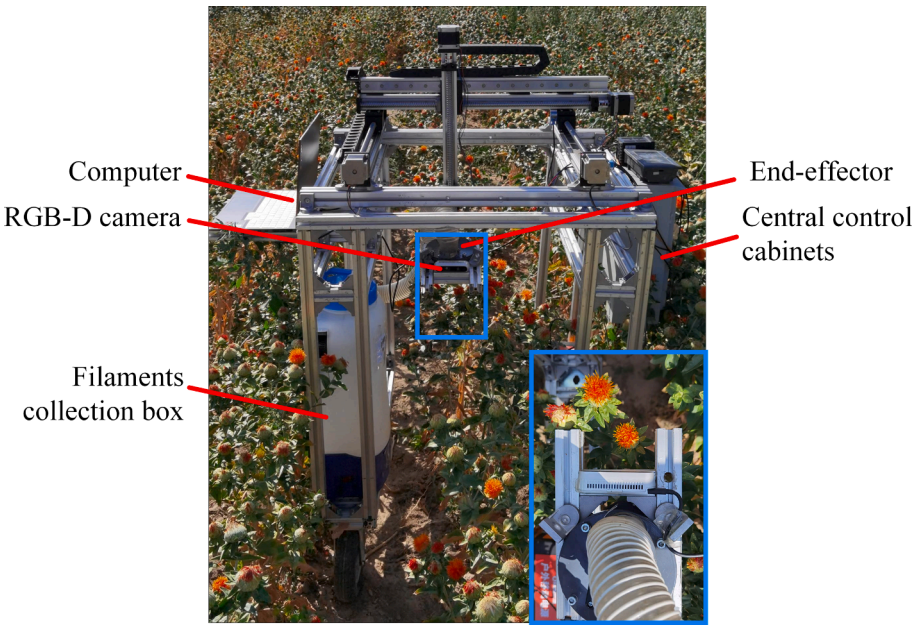

Fig. 1. Safflower-picking robots collecting images in the fields.

Fig. 2. Images of different types of safflower: (a) sunny day with light, (b) sunny day with backlight, (c) overcast day with light, and (d) cloudy day with light.

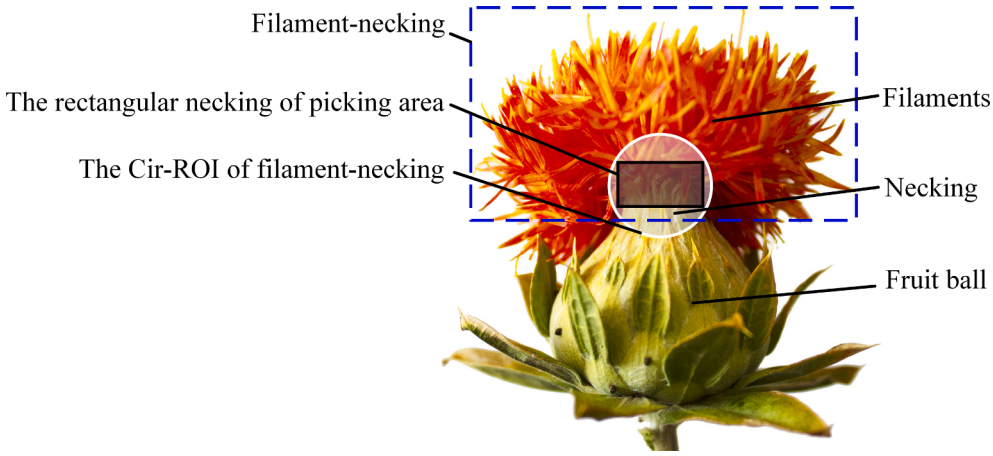

Fig. 3. Structure diagram of the opening safflower.

velocity and position are adjusted appropriately to adapt to the scenes. Therefore, according to the position, speed, and experience function updating of filaments, the improved PSO algorithm performs a global search of the safflower image and quickly searches to locate the filaments. Then, the redesigned adaptation function is used to dynamically adjust the optimization search. The global search of filaments is locally converged on edges and non-edges to maximize the extraction of intact filaments. Making the population update the historical optimal adaptation value and position, the safflower filaments are segmented with the best results.

(1) Velocity and position update function

Since the target safflower filaments of the image are close in color to the other safflowers illuminated by the strong light, it makes less difference in the grayscale value of the image. The PSO algorithm search strategy is used to guide the search through the global optimal position and individual optimal position (Wang et al., 2022). To search the global

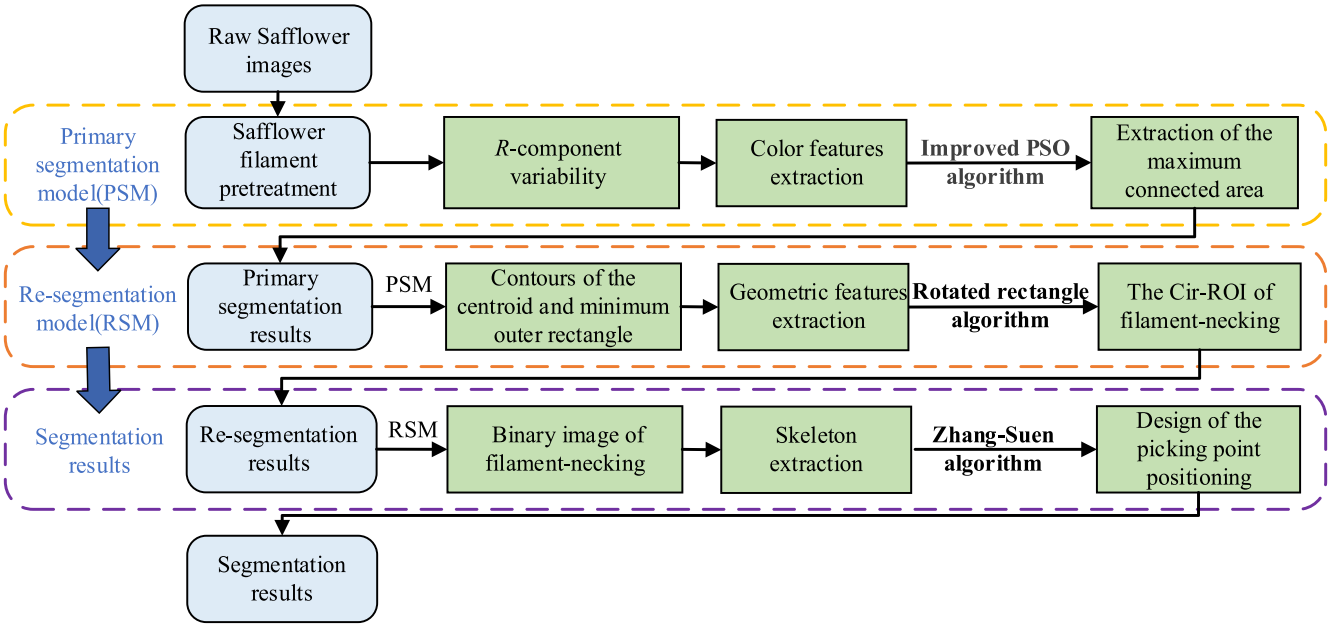

Fig. 4. Flow of the filament-necking localization method for safflower-picking robots.

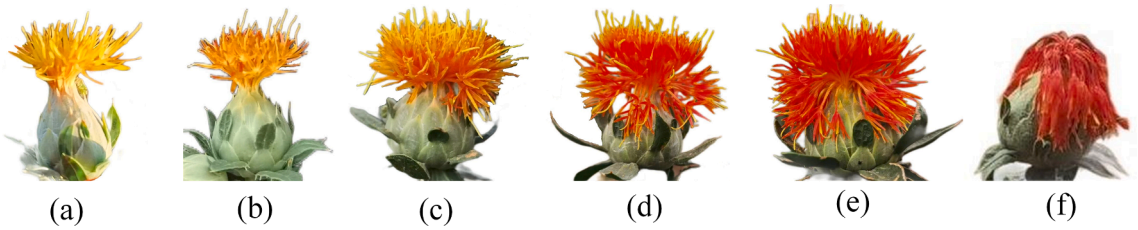

Fig. 5. Color change of filaments after opening on different days: (a) 1st day, (b) 2nd day, (c) 3rd day, (d) 4th day, (e) 5th day, and (f) 6th day.

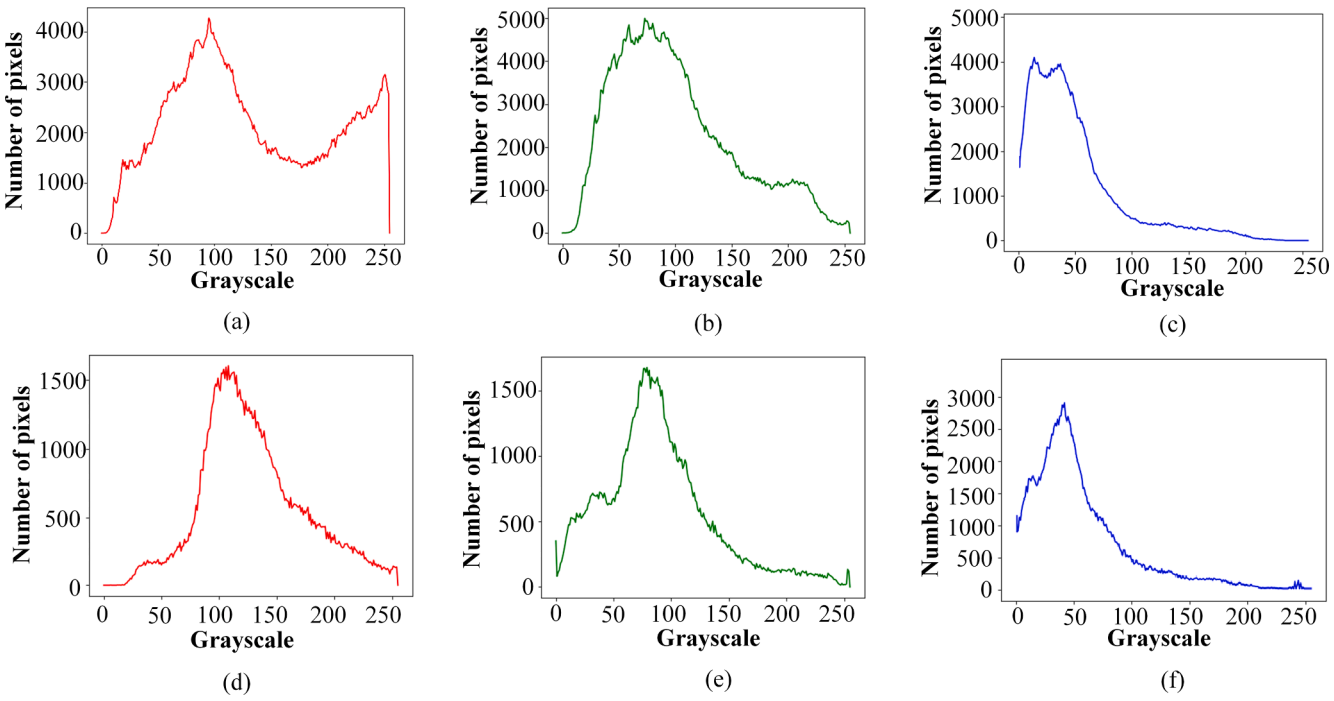

Fig. 6. Histogram of RGB components of safflower images in opening for 4–5 days: (a), (b), and (c) are the R, G, and B component histograms in the opening period, respectively. (d), (e), and (f) are the R, G, and B component histograms in the flower-shedding period, respectively.

safflower position quickly, the particle swarm optimization search strategy is used for global position optimal search.

The speed update function is shown in Eq. (1):

$$v_e^k = \omega v_e^{k-1} + c_1 r_1 \left(x_p^{k-1} - x_e^{k-1}\right) + c_2 r_2 \left(x_g^{k-1} - x_e^{k-1}\right) \tag{1}$$

where v_e^k denotes the current kth iteration particle e velocity; w denotes the inertia weight; c_1 and c_2 denote the acceleration constants; r_1 and r_2 denote two stochastic functions with values in the range of [0, 1]; x_p^{k-1} denotes the historical optimal position of particle e in the kth iteration; x_g^{k-1} denotes the historical optimal position of the population in the kth iteration.

The position update function is shown in Eq. (2):

$$x_e^k = x_e^{k-1} + v_e^{k-1} \tag{2}$$

where x_e^k denotes the position of particle e after updating in the kth iteration.

(2) Design of nonlinear functions for inertia weights.

As the global safflower is interfered with by many external factors, the safflower images have a complex background environment. Consequently, the accuracy of the local search for the target safflower filaments edges is reduced after the global search. The unsatisfactory segmentation effect affects the subsequent re-segmentation and localization results of the picking point. Therefore, considering that the value of inertia weight ω affects the performance of PSO, the inertia weight ω nonlinear function is redesigned with the PSO algorithm and the characteristics of safflower filaments.

Larger values of the inertia weights ω are associated with strong global optimization search and weak local optimization search. Conversely, the local optimization ability is powerful. To achieve a balance between search speed and search accuracy, the algorithm has a high global search ability in the early stage to obtain suitable particles. At the later stage, there is a high local search ability to improve the convergence accuracy. It means that the inertia weights ω decreases nonlinearly with the increase in the number of iterations. Larger inertia weights ω have better global convergence ability, while smaller inertia weights ω have stronger local convergence ability. Currently, most algorithms set the inertia weights to decrease linearly with the increase of iterations (Singh et al., 2021b; Sabzi et al., 2019; Zou et al., 2022). However, the linearly decreasing strategy does not work well for dynamic systems. Therefore, a dynamic inertia weight strategy that decreases nonlinearly with the number of iterations is proposed.

The improved inertia weights ω nonlinear function is shown in Eq.3:

$$\begin{cases} \omega_{\min} + \dfrac{\omega_{\max} - \omega_{\min}}{e^{-\omega_{\max}} + e^{-C+50\frac{T}{T_{\max}}}}, 0 \le C < \dfrac{T}{T_{\max}} \le 0.5 \\ \omega_{\max}, \text{otherwise} \end{cases} \tag{3}$$

where $\omega_{\max}$ denotes the maximum value of inertia weights ω, $\omega_{\min}$ denotes the minimum value of inertia weights ω, C denotes a random constant, T denotes the current iteration step, and $T_{\max}$ denotes the maximum number of iterations, 50 denotes the iteration constant, which is obtained from the previous experiment.

(3) Design of the fitness function

To enhance the difference between the grayscale of the safflower filaments and the branch leaves or other filaments, the same fitness function is used to avoid the disadvantage that the algorithm tends to fall into local extremes. The collected images are processed separately using the grayscale operator represented by each particle in the population. The mean difference and grayscale images variance of the safflower filaments, branches or leaves, and other filaments are used as evaluation indexes.

When the local size of safflower filaments images is $M \times N$, the window center coordinates are (m, n). The mean difference is more beneficial to the grayscale of images. It is calculated as shown in Eq. (4).

$$E = \frac{1}{MN} \sum_{i=-\frac{M}{2}}^{\frac{M}{2}-1} \sum_{j=-\frac{N}{2}}^{\frac{N}{2}-1} h(m+i, n+j) \tag{4}$$

where E denotes the grayscale of images, and $h\,(m+i, n+j)$ denotes the gray value of the image to be segmented.

When the grayscale standard deviation s' is smaller, it is more beneficial to grayscale the image of safflower filaments. The calculation is shown in Eq. (5).

$$(s')^2 = \frac{1}{M(N-1)} \sum_{i=-\frac{M}{2}}^{\frac{M}{2}-1} \sum_{j=-\frac{N}{2}}^{\frac{N}{2}-1} [h(m+i, n+j) - E]^2 \tag{5}$$

where s' denotes the standard deviation in the local neighborhood.

Localization of the picking point needs to meet the picking demand with the shortest time and fastest localization (Benbarrad et al., 2021). When designing the fitness function, the minimum error and running time of the optimization PSO algorithm should be considered comprehensively to improve localization accuracy. To integrate E and s' with large differences, the logarithm and reciprocal of each object are calculated to add up to obtain the objective function. The larger fittingness function value indicates that the individual is more optimal. The specific design process of the fitness function is shown in Eq. (6).

$$f(x) = \frac{1}{\lg(E)} + \frac{1}{\lg(s')^2} \tag{6}$$

The safflower filaments were processed using the grayscale operator to obtain the grayscale map of filaments ROI (Xiang, 2018). However, using the OTSU (Gao and Lin, 2018) and iterative algorithm (Almoujahed et al., 2022), the segmentation results were often caused by mis-segmentation cases, such as burrs, isolated points, and partial scattering noise due to thresholding errors. Consequently, the noise filtering operation of safflower images was cumbersome and occupied a long time. However, the improved PSO algorithm could cope with different noises in the safflower filament images and realize the adaptive threshold value. Meanwhile, the time of manually setting the threshold value was saved in the detection process, so that the improved PSO algorithm could be better utilized in practical production. Therefore, the maximum number of iterations was set to 50 as the termination condition of the algorithm. Using the improved PSO algorithm to the grayscale of ROI, the binary image of safflower filaments with less noise was segmented.

After image segmentation, there were still some noises (burrs, isolated point, and partial scattering noise) in the segmented image. The binary image was denoised and filled using a closed operation followed by an open operation. Then the closed operation could effectively remove the burr and isolate noise caused by the thresholding error, and could also cause the formation of some obvious holes in the crop (Liu et al., 2016). However, the open operation could be filled with holes (Granland et al., 2022). Moreover, the binary image of the maximum connected region for the safflower filaments was retained. The effects of the morphological treatment are shown in Fig. 7.

3.3. Re-segmentation based on geometric features

To improve the accuracy of localization and the preservation of intact filaments, removing the image noise affected the localization of the picking point to the features of the diversity in safflower growth. The Cir-ROI of filament-necking was selected. When calculating the picking point, only the images within the Cir-ROI were processed. Reducing interference in localization caused by image regions that are not related to the picking point solution (Ulzii-Orshikh et al., 2017).

3.3.1. The barycenter and minimal outer rectangle of safflower filaments

Barycenter is the geometric center of safflower filament images.

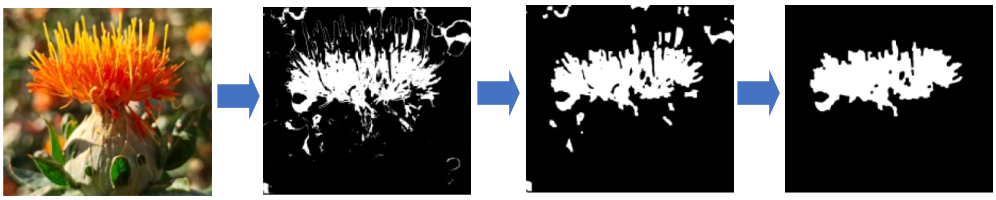

Fig. 7. The process of safflower filaments images segmentation: (a) original image, (b) binarization, (c) morphological arithmetic, and (d) the maximum connected area.

Combined with section 3.2.3 to obtain the binary image, the barycenter point of safflower filaments was solved for the binary image according to the definition of barycenter moments. The barycenter coordinates (x_c, y_c) were obtained. The calculation is shown in Eq. (7).

$$\begin{cases} x_c = \sum xf(x,y) / \sum f(x,y) \\ y_c = \sum yf(x,y) / \sum f(x,y) \end{cases} \tag{7}$$

Where x_c denotes the barycenter horizontal coordinate of the image; y_c denotes the barycenter vertical coordinate of the image; x,y denote the pixel coordinates; and $f(x,y)$ denotes the pixel value of the binary images at point (x,y).

For the inclined growth of safflower filaments, the filament-necking localization method adopted the rotating rectangle algorithm based on the features of geometric features. After obtaining the barycenter coordinates, the left, right, up, and down extreme value lines were solved for the maximum connectivity region. Based on the contour boundary of the extreme point, the smallest rectangle containing the contour point was located. Then, the center and angle of the rectangle were used to define the rotation rectangle to accommodate the inclined growth feature. Thus, the minimum outer rectangle contained more pixel point of the target. According to the minimum outer connecting rectangle and barycenter coordinates, the ROI of the safflower filament and the maximum left and right lengths of the bottom edge L_{max} were output on the original map, as shown in Fig. 8.

3.3.2. Determination of the Cir-ROI

To decrease the difficulty of segmentation and ensure the validity of the picking point, the Cir-ROI of filament-necking was determined based on the barycenter and the minimum outer rectangle. Given the small horizontal difference between the horizontal coordinates of the filaments barycenter and the horizontal coordinates of the necking rectangle center, the maximum length of the bottom edge for the minimum outer rectangle L_{max} passed through the region of the necking rectangle picking. Therefore, the horizontal coordinate x_3 of the center point of the Cir-ROI was selected as the horizontal coordinate x_1 of the filament barycenter, and the vertical coordinate y_3 was selected as the vertical coordinate y_2 of the midpoint of the bottom edge of the minimum outer rectangle.

However, the rectangular necking of the picking area was small in both length and width relative to the safflower filaments. There was a certain offset for the center of the Cir-ROI. Both of them would lead to the partial exclusion of the rectangular necking of the picking area. To make the Cir-ROI of filament-necking retain more of the rectangular necking of the picking area and the division more obvious, the circular radius was divided into two cases based on the relevant data on filaments width, height and necking in Table 1. (i) When the difference between the longitudinal coordinates of filament barycenter y_1 and the longitudinal coordinates of the smallest outer-connecting rectangle midpoint y_2 were less than or equal to L_{max}, the circular radius was adopted by taking 2/3 of the difference of both, as shown in Fig. 9a. (ii) When the difference was greater than L_{max}, the adoption of the circular radius took 1/6 of the maximum left and right length L_{max}, as shown in Fig. 9b. The calculation is shown in Eq. (8).

$$r = \begin{cases} \frac{2}{3}|y_1 - y_2|, |y_1 - y_2| \le L_{max} \\ \frac{1}{6}L_{max}, |y_1 - y_2| > L_{max} \end{cases} \tag{8}$$

where r denotes the radius of the Cir-ROI; y_1 denotes the longitudinal coordinate of the center of filament barycenter; y_2 denotes the longitudinal coordinate of the highest point in the minimum outer rectangle of the safflower filament; and L_{max} denotes the maximum left and right length of the bottom edge in the minimum outer rectangle.

3.4. Localization of picking point

Obtaining information on the exact location of the safflower-picking point can decrease the breakage rate of filaments and retain their integrity. After determining the Cir-ROI, the information on the necking was used in image segmentation and morphology of section 2.3.2 processing methods to obtain the exact position information of the safflower-picking point. Using the open or close operation and the filling algorithm employed to trim the edge burrs of the image and fill in the effective region of the necking that had been segmented incorrectly, the grayscale images were converted to a binary image. Further, the subtraction operation of the binary image was done to get the necking binary image, as shown in Fig. 10 (a)and Fig. 10 (b). Having preprocessed

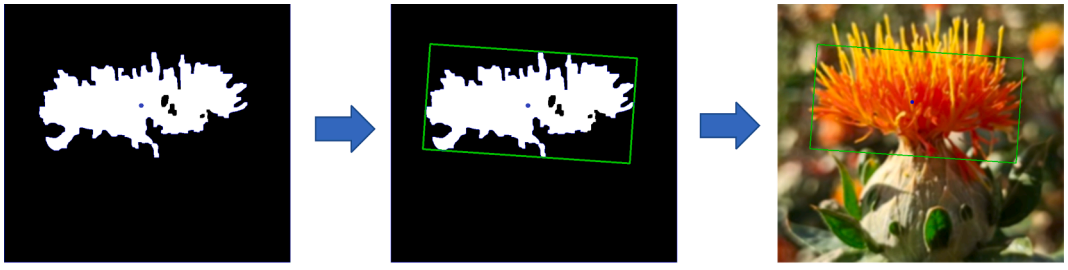

Fig. 8. Morphological parameters of safflower filaments image: (a) safflower filaments bivalent image, (b) safflower filaments barycenter and minimal outer rectangle, and (c) safflower filaments original image markers.

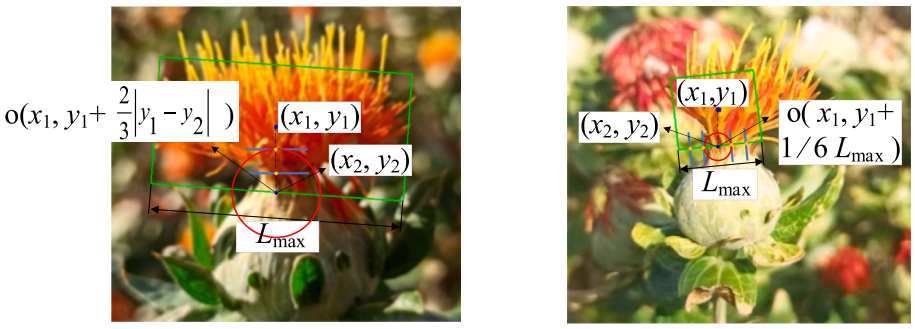

(a) (b)

Fig. 9. Determination of Cir-ROI: (a) $|y_1 - y_2| \leq L_{max}$, and (b) $|y_1 - y_2| > L_{max}$.

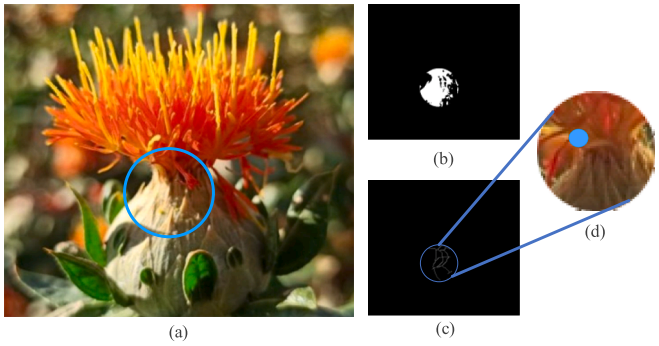

Fig. 10. The localization process of picking point: (a) the Cir-ROI of filament-necking, (b) color component binary image of Cir-ROI, (c) extraction of the necking skeleton, and (d) calculated picking point.

the Cir-ROI of filament-necking, the necking skeleton needed to be extracted and localized. The Zhang-Suen refinement algorithm (Leborgne et al., 2015; Janković, 2022) was used to make its pixel width smaller and refine the necking as a whole. Furthermore, the remaining pixel point was composed of the connective skeleton. The obtained image of the skeleton was beneficial in determining the location of the picking point, as shown in Fig. 10 (c).

Since the skeleton is mostly distributed in disordered vertical lines, the filament-necking localization method was conducted by traversing the entire binary image of the necking skeleton. The main purpose was to search for the smallest value of the horizontal and vertical coordinate pixel point in the binary image of the skeleton. The smallest value was determined as the picking point, as shown in Fig. 10 (d). The minimum horizontal coordinate x pixel value was set as the horizontal coordinate of the picking point. The minimum vertical coordinate y pixel value was set as the vertical coordinate of the picking point. The result of the calculation was used as the safflower-picking point. Meanwhile, the picking point was marked with a solid blue circle. The picking point calculation formula is shown in Eq. (9).

$$\begin{cases} F_x = G_x \\ F_y = G_y \end{cases} \tag{9}$$

where F_x and F_y are the horizontal and vertical pixel values of the picking point, respectively; and G_x and G_y are the minimum horizontal pixel value and minimum vertical pixel value obtained by traversing the neckdown skeleton, respectively.

4. Experimental setup

4.1. Test platform

The test platform was chosen as follows: (i) the safflower-picking robots were mainly composed of a computer, a central control cabinet, an RGB-D camera, a filament collection box, and an end-effector; (ii) a software environment with Windows 11 system, and a python 3.8.8 development environment using the Visual Studio Code software for compilation and analysis; (iii) a computer with the hardware configuration of Intel(R) Xeon(R) Silver 4116 CPU@2.10 GHz, 64 GB RAM, and NVIDIA Quadra P5000 graphics card; (iv) RGB-D Camera with Intel RealSense D435 camera.

4.2. Evaluation indicators

In the testing session, 400 test images of safflower were detected using the filament-necking localization method. Meanwhile, four aspects are compared in terms of segmentation correctness, running time, and accuracy of picking point.

(1) Average relative target area error rate.

To objectively evaluate the effectiveness of the segmentation method proposed, the average relative object area error rate was chosen to quantitatively evaluate the quality of safflower extraction (Wang et al., 2019b). The calculation is shown in Eq. (10).

$$R_r = \frac{\sum_{i=1}^{N} \left| \frac{A_1 - A_2}{A_1} \right|}{N_c} \times 100\% \tag{10}$$

where i denotes the ith test image, N_c denotes the number of test images, A_1 denotes the area of the target region in the actual safflower image, and A_2 denotes the area of the target region in the test image.

The area of the target region in the actual safflower image was obtained manually by manual segmentation through Photoshop, and the area of the target region was expressed in terms of the number of pixels in the region. The number of pixels was obtained through Visual Studio Code software.

(2) Average running time.

The average running time t (Wang et al., 2019b) is defined as shown in Eq. (11).

$$t = \frac{t_a}{N_c} \tag{11}$$

where t_a is the total elapsed time for recognizing N_c images to be tested.

(3) Accuracy of picking point.

To analyze the accuracy of picking point localization, pixel localization error was used as the main index (Luo et al., 2015), as shown in Eq. (12).

$$\begin{cases} e = \sqrt{\left(e_x^2 + e_y^2\right)} \\ e_x = \min|X - x| \\ e_y = \min|Y - y| \end{cases} \tag{12}$$

Where X and Y denote the pixel region of the optimal picking point; x and y denote the pixel coordinates of the picking point obtained by the present method; e_x and e_y denote the row and column direction errors of the obtained picking point to the pixel region of the optimal picking point, respectively; and e denotes the total pixel localization error of the obtained picking point.

(4) Intersection Over Union

To test the performance of the proposed algorithm, the Intersection Over Union (IOU, %) is chosen as an index to evaluate the effectiveness of the model, as shown in Eq. (13):

$$\text{IOU} = \frac{\text{area}(A_P \cap A_T)}{\text{area}(A_P \cup A_T)} \tag{13}$$

where A_P is the predicted value; A_T is the true value; and IOU is the overlap between the safflower predicted bounding box and the safflower true bounding box.

5. Experimental results

5.1. Comparison of different segmentation methods

To verify the adaptability and effectiveness of the improved PSO in complex backgrounds, 400 images of safflower under different weather lighting are detected. The typical detection results are shown in Fig. 11. The segmentation results are compared with the segmentation results of the OTSU algorithm, iterative algorithm, CDMS segmentation algorithm (Zhou et al., 2022), CondInst segmentation algorithm (Tian et al., 2022), and MDE-UNet (Wang et al., 2023) to assess the various performances of the algorithm.

The OTSU algorithm segmentation was a commonly used image segmentation method (Gao and Lin, 2018). However, the complexity of the safflower filaments background, coupled with changes in light intensity, made the target safflower filaments similar to the background color. The segmentation effect of the iterative algorithm was similar to the segmentation effect of the OTSU algorithm. Both of the results were prone to large-area mis-segmentation and worse segmentation effects. Occasionally, the phenomenon of greater noise occurs. In addition, the CDMS, CondInst, and MDE-UNet, which were currently used in top journals, still had serious background segmentation for safflower filaments with complex backgrounds. For example, CDMS and CondInst segmentation algorithms had poor segmentation effects due to the high similarity of color and morphological features caused by the large variation of illumination. MDE-UNet also had the problem of large noise and large segmentation errors, which could not completely segment safflower filaments. According to the related segmentation algorithm (Almoujahed et al., 2022), the main reason for the poor segmentation effect was that the use of iterative or OTSU algorithm of grayscale image segmentation, resulting from the target filaments and the color of the background was close to making the three grayscale value differences was not large. Therefore, there was no obvious “bimodal peak” in the grayscale histogram, resulting in a worse segmentation effect of the iterative or OTSU algorithm.

Compared with the segmentation results of the OTSU and iterative algorithm, the safflower region of the grayscale processed was enhanced with the optimization of a method by the improved PSO algorithm. The improved PSO algorithm could accurately segment the safflower filaments from the complex background of other filaments, and strongly illuminated leaves, as shown in Fig. 11. Meanwhile, the improved PSO algorithm could be more effective in overcoming the influence of strong light brought about by non-uniform illumination. Excellent segmentation results were still achieved under cloudy day with light conditions.

Fig. 12 shows the performance indicators of different methods for segmenting images in Fig. 11.

Fig. 12 demonstrates the average relative target area error rate and average running time of different methods for image segmentation under four conditions. The iterative segmentation and OTSU algorithm mistakenly segmented other filament regions and the background region of strongly illuminated branches and leaves as filaments. The area of the target safflower filaments region of the test image was larger than the area of the actual, resulting in a low average relative target area error

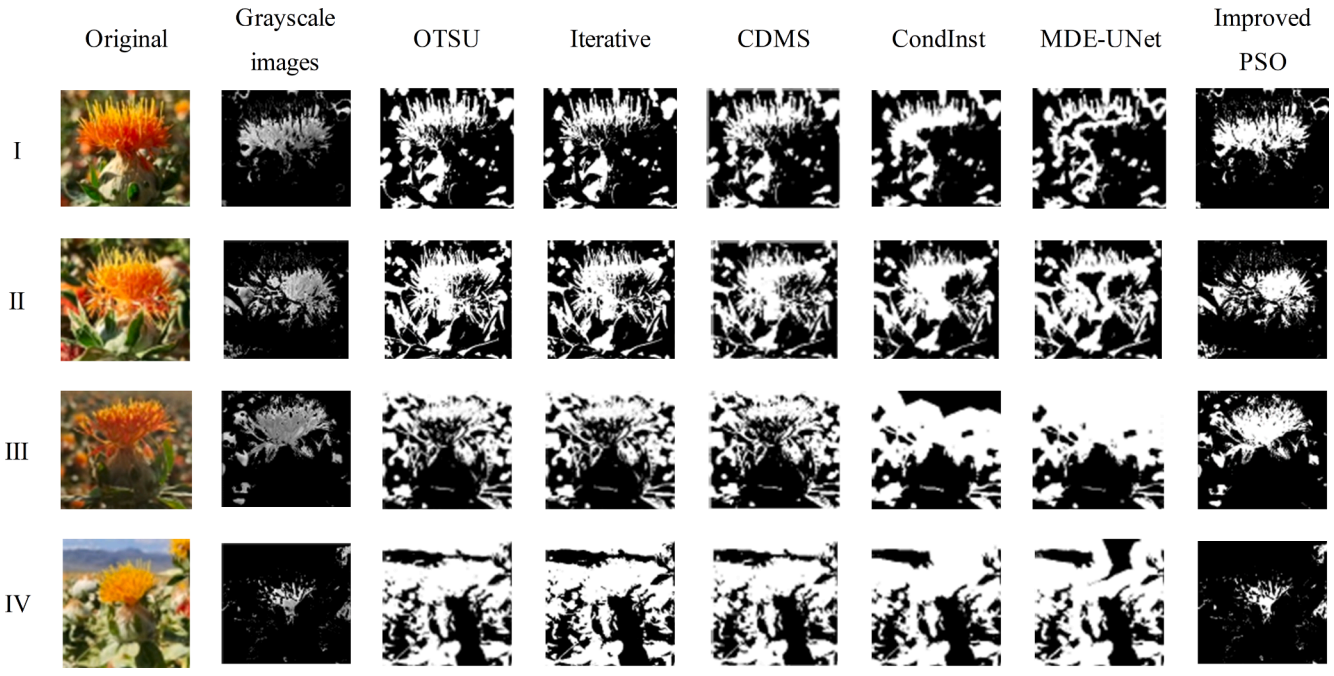

Fig. 11. Grayscale and segmentation results of safflower images under different weather conditions I. sunny day with light, II. sunny day with backlight, III. overcast day with light, and IV. cloudy day with light.

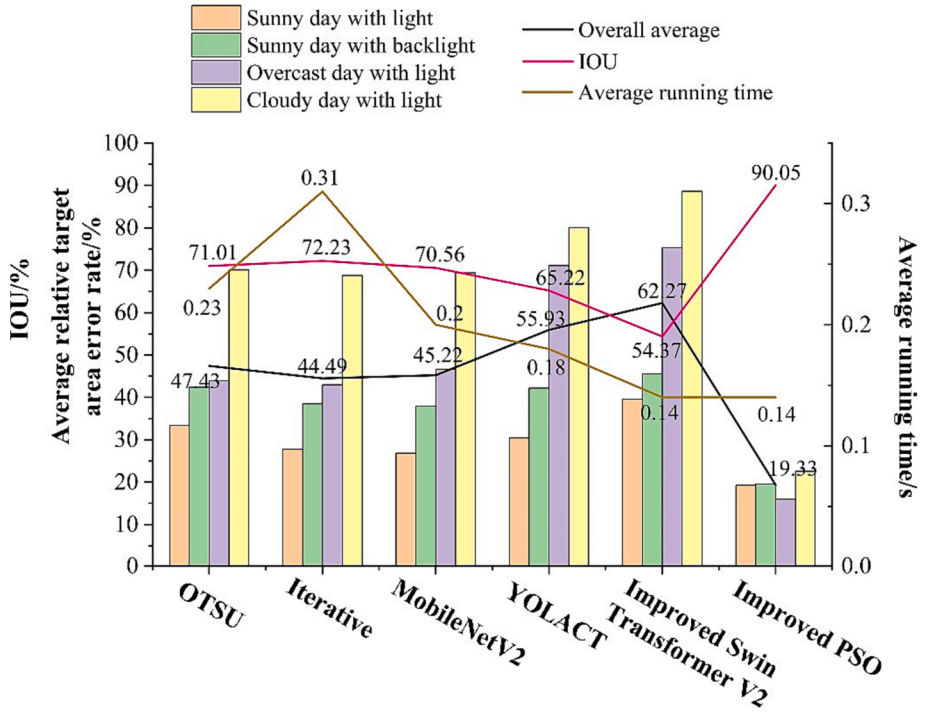

Fig. 12. Performance indicators of different algorithms for segmenting images.

rate. The OTSU, iterative, CDMS, CondInst, and MDE-UNet algorithms were 47.43 %, 44.49 %, 45.22 %, 55.93 %, and 62.27 %, respectively.

From the average index of segmentation performance, a sunny day with light had better segmentation results than a sunny day with backlight, with a maximum difference of 11.76 %. An overcast day with light had better segmentation results than cloudy day with light, with a maximum difference of 26.13 %. It was shown that the lighting conditions influenced the segmentation of the 5 algorithms. From the overall situation, the filament-necking localization method had better segmentation results under sunny day with light and backlight conditions. Segmentation effects were well under a sunny day with light and backlight conditions, but an overcast day with light was better than a cloudy day with light for segmentation. The average relative target area error rate was lower by 6.56 %. The improved PSO algorithm had the lowest average relative target area error rate among the 5 algorithms, with 28.1 %, 25.16 %, 25.89 %, 36.60 %, and 42.94 % lower than the OTSU, iterative, CDMS, CondInst, and MDE-UNet algorithms, respectively.

From the IOU index, the IOU value of the improved PSO algorithm was significantly higher than the other 5 algorithms by more than 17.82 %. The reason was mainly that the background of the safflower filament was complex and variable, and the surrounding branches, leaves, and filaments were extremely similar to the filament color and texture features. The improved PSO algorithm utilized the improved PSO for local search and convergence, and more finely segments the filaments, but the other 5 algorithms showed worse local convergence and segmentation ability.

From the time indicators, the average running time on 400 images, improved PSO algorithm spent less time relative to the OTSU and the iterative algorithm. The average processing time of the improved PSO algorithm was lower than the OTSU, iterative, CDMS, and CondInst algorithms by 0.09 s, 0.17 s, 0.06 s, and 0.04 s, respectively. The average relative target area error rate was lower than the iterative algorithm segmentation and the OTSU algorithm segmentation. The average running time was the same as that of MDE-UNet, but its average relative target area error rate and IOU were significantly lower than that of the improved PSO algorithm.

5.2. Picking point localization algorithm

To demonstrate the effectiveness of the method, the performance of the picking point localization algorithm proposed in this study is evaluated by two metrics: precision and recall. The precision and recall are defined as follows:

$$Precision = \frac{TP}{TP + FP} \tag{14}$$

$$Recall = \frac{TP}{TP + FN} \tag{15}$$

Where *TP* is the number of correctly identified picking points, *FP* is the number of incorrectly identified picking points, *FN* is the number of unidentified picking points.

There have been many studies on picking point localization in crops. To verify the effectiveness of the proposed algorithms, the three latest picking point localization algorithms are selected for discussion. If the localized picking point was located in the necked rectangular picking area corresponding to safflower filaments, the localization was considered successful. Otherwise, it was judged as a localization failure. The 400 images under four weather conditions were tested. The comparison of relevant performance metrics is shown in Table 2.

MobileNetV2 (Li et al., 2023a,b) mainly utilized the algorithm to obtain the contour key points and necking key points of safflower filaments. Through the effective prediction of these two key points, the picking point was obtained. YOLACT (Zhong et al., 2021) performed skeleton extraction based on the mask of the necking and then used the least squares method to fit the necking spindle to calculate the picking

Table 2
Localization performance test results of the four models.

Literature	*TP*	*FP*	*FN*	*Precision/%*	*Recall/%*
MobileNetV2	234	80	86	74.52	73.13
YOLACT	287	57	56	83.43	83.67
Improved Swin Transformer V2	301	39	60	88.53	83.38
Improved PSO	368	11	21	97.10	94.60

point. Improved Swin Transformer V2 (Rong et al., 2023) determined the ROI of the necking and performed the edge detection and the cumulative probability Hough transform on the necking. The final picking point was determined based on the relationship between necking and filaments barycenter. The improved PSO algorithm was to determine the Cir-ROI of filament-necking and search for the value with the smallest coordinate pixel point in the binary image of the skeleton, which was determined as the picking point. As shown in Table 2, the algorithm proposed in this study performs best on the filament dataset with the highest precision and recall, 97.10 % and 94.60 %, respectively. However, MobileNetV2 had a poor performance on the filament dataset. The main reason was the poor accuracy of detecting necking and the use of a crude picking point localization method. YOLACT and Improved Swin Transformer V2 showed relatively improved localization results, with 8.91 %, 10.54 %, and 14.01 %, 10.25 % improvement in precision and recall, respectively. The main reason was that the two algorithms paid attention to the intrinsic relationship between necking and picking points. Nevertheless, they hadn't paid attention to the complex and changing background of the image, and the small area of necking, which was still poorer compared to the localization effect of the improved PSO algorithm.

5.3. Localization results of picking point

The 400 test images of safflower were selected for validation under four weather conditions, including 100 images each under different weather conditions. During the picking point localization, the Cir-ROI of filament-necking, skeletonization, and localization results are shown in Fig. 13.

Using the filament-necking localization method, the pixel coordinates of the barycenter and the picking point of the 400 test images were calculated under four different weather conditions. The necking rectangular picking area (160 × 80 pixels) was used as the localization of the optimal picking point, for calculating the error between the picking point and optimal picking point. Table 3 shows the results of the picking point and pixel localization error for the four images in Fig. 12.

Table 3 demonstrates the coordinates/pixel of the safflower barycenter and picking point, and the error/pixel from the optimal picking point under different weather conditions. The testing results show that the pixel error from the optimal picking point is less in the X (row) direction. When the obtained picking point x-value is within the range of X, the e_x was 0. However, there were 2 to 8 pixel errors between the optimal picking point and the optimal picking point in the Y (column) direction.

The filament-necking localization method had no error between picking points/pixels and optimal picking points under a sunny day with backlight. Meanwhile, the terms of localization accuracy were slightly better than the smooth light. The reason lay in the change in lighting conditions. Backlighting improved the light intensity and brightness on the safflower images and weakened the background color overlap caused by strong light. It was more beneficial localization for picking point. However, the error between the obtained picking point and the optimal picking point under a sunny day with light was 4 pixels more than under a sunny day with backlight. Sunny day with light increased light intensity and brightness in the safflower images. Because the safflower filaments themselves blended with the complex surrounding environments, especially other safflower filaments, the different color of the localization safflower was the same as the surrounding background. In addition, when incomplete extraction of the safflower image resulted

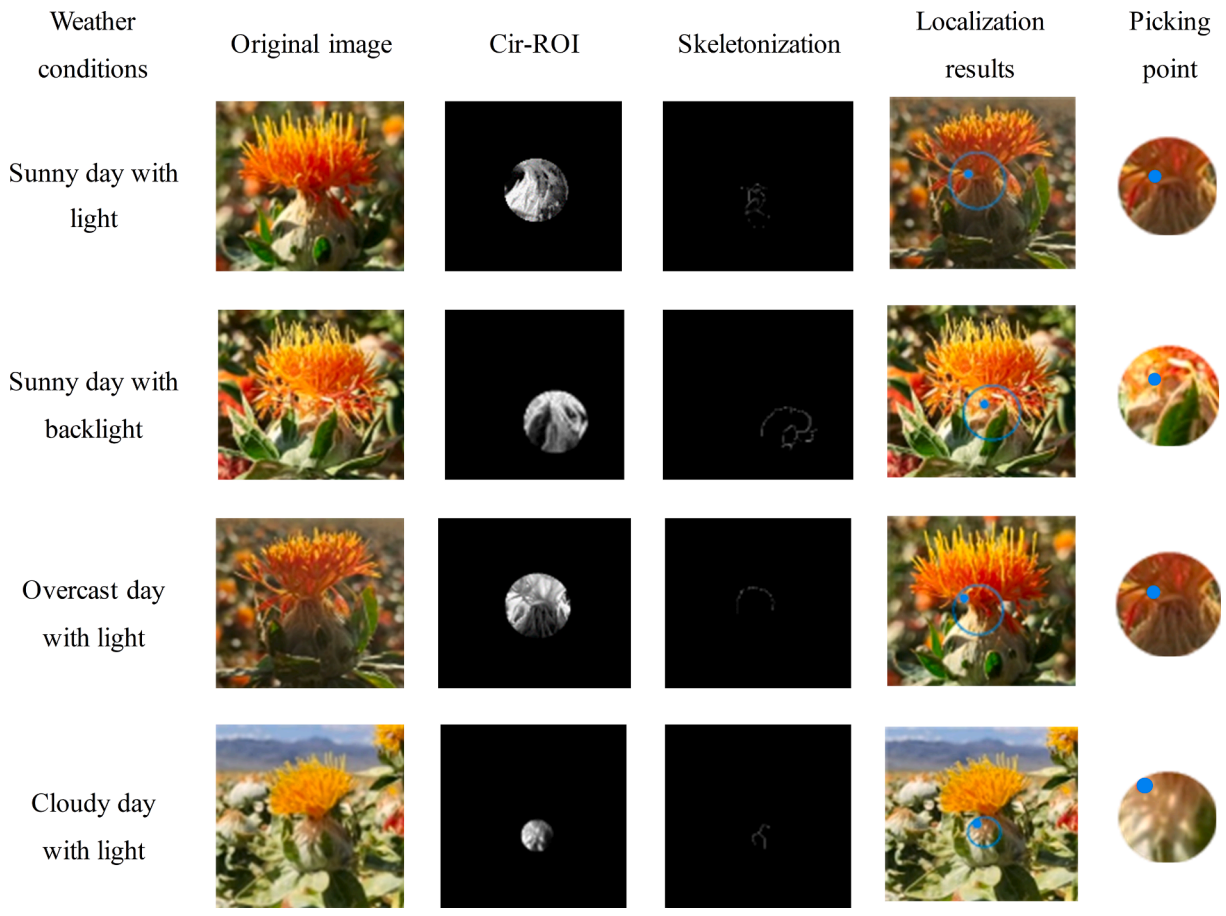

Fig. 13. Localization process of picking point under 4 weather conditions.

Table 3
Picking point and pixel localization errors.

Weather conditions	Barycenter coordinates/pixel		Optimal picking point range/pixel		Obtain the picking point/pixel		Error/pixel from optimal picking point			Radius
	X_3	Y_3	X	Y	x	y	e_x	e_y	e	r
Sunny day with light	370	271	313 ~ 463	348 ~ 428	317	344	0	4	4	172
Sunny day with backlight	319	190	201 ~ 361	220 ~ 300	237	250	0	0	0	127
Overcast day with light	220	135	198 ~ 348	157 ~ 237	198	192	0	0	0	167
Cloudy day with light	221	194	186 ~ 336	200 ~ 280	188	231	0	6	6	63

in too large an error in the computation of the barycenter, the localization of the picking point led to a bias.

Pixel localization error statistics were performed on 400 test images. The error distribution is shown in Table 4.

Combined with the filament-necking localization method in skeletonizing the Cir-ROI of filament-necking, the detection was usually based on the morphological features of the crop. The detected line segments were located at the edge of the indented neck. When the Y-direction was prone to pixel error, the calculated picking point had $e \geq 8$ pixels. The different weather lights affected the safflower color difference. It resulted in the proportion of Cir-ROI satisfying localization with sunny and cloudy day with light being 88 % and 83 %, respectively. Both of them were lower than that of sunny backlight and cloudy day with light both exceeding 5 %, and the average running time was more than 0.20 s. Therefore, the Cir-ROI of filament-necking had to satisfy the localization requirement by picking a point within the rectangular picking area of the necking rectangle. Meanwhile, the picking point needed to satisfy $e < 8$ pixels. The reason was mainly that the backlight on a sunny day was relatively soft in brightness due to low light intensity. The highest proportion of Cir-ROI satisfying localization was 95 % under sunny days with backlight conditions. Therefore, combining the picking point localization results of 400 test images, the overall localization accuracy of the picking point was 89.75 %.

In addition, overcast day with light had better recognition accuracy than cloudy day with light. Because of the weaker light intensity on overcast days with light, the color of the necking part is highlighted in the Cir-ROI of filament-necking stand out. Simultaneously, there was less irrelevant information, so the localization of the picking point was less prone to bias. In contrast, cloudy day with light was often accompanied by changes in light and was unstable in light intensity. Therefore, the rectangular necking of the picking area was difficult to distinguish, leading to a large deviation in the localization of the picking point.

5.4. Field experiments

The picking robot for the field experiments was based on an *XYZ* 3-axis sliding module as platform, end-effector as picking device, and an RGB-D camera as vision core, as shown in Fig. 14 (a). The method proposed in this study was verified in the field environment. Fifty field experiments were conducted under the conditions of sunny day with light, sunny day with backlight, cloudy day with light, and cloudy day with light, respectively. The results of camera localization for picking point are shown in Fig. 14 (b). In addition, the breakage rate of filaments was the percentage of the weight of broken and shattered filaments in a single safflower picked as compared to the total weight of the picked filaments. The results of filaments picking after localization are shown in Fig. 14 (c).

Table 4
Localization of picking point under 4 weather light conditions.

Weather conditions	Original image/frame	$e < 8$ pixels	Percentage of Cir-ROI that satisfy localization	Average running time/s
Sunny day with light	100	88	88	0.205
Sunny day with backlight	100	95	95	0.171
Overcast day with light	100	93	93	0.188
Cloudy day with light	100	83	83	0.229

The localization data are shown in Table 5. The results showed that the highest success rate of 93 % was achieved in locating safflower filament harvesting points under sunny backlight conditions. The analysis showed that safflower filaments under cloudy light were affected by light and other objects shading, resulting in blurring of the color and texture characteristics of the filaments. The localization success rates of the filament picking point were lower than 2 % under other weather conditions, the breakage rates of filaments were higher than 0.54 %, and the average running times were higher than 0.025 s.

6. Discussion

Compared with the other visual localization methods (Gongal et al., 2015a) with worse resistance to background noise and large localization error, the filament-necking localization method had the following characteristics. (i) The PSO algorithm was improved to enhance the global and local search capability. The interference of the background region was effectively reduced on safflower filament detection. (ii) The Cir-ROI of filament-necking was re-segmented with a rotated rectangle algorithm. The problem of picking point localization error was mitigated due to variations in light intensity and plant shading. (iii) Analysis of safflower features was introduced to combine the primary segmentation and re-segmentation results. Using skeleton extraction to determine reasonable picking point locations suppressed effectively the background noise from mixing into the re-segmentation results.

The experimental results have shown that the segmentation results obtained with the filament-necking localization method were closer to the real safflower image than other methods. The average processing time of the improved PSO algorithm was lower than the OTSU and the iterative algorithm by 0.09 s and 0.17 s, respectively. The average relative target area error rate was lower than the OTSU method by 28.10 % and the iterative method by 25.16 %. Meanwhile, the Cir-ROI of filament-necking satisfied the localization were all above 80 %. In addition, the localization accuracy of the picking point reached 88.33 %. The filament-necking localization method was adaptable to different weather light changes. In the comprehensive analysis, the positioning accuracy of the picking point was higher under sunny and cloudy day with light conditions. In particular, the backlight localization on sunny days was the best, reaching 95 %. Although the filament-necking localization method was designed for safflower, the method is informative for image segmentation of a single target under a complex background and similar crop picking in the target area.

In the process of safflower filaments picking, the current method mainly solves the single filaments. However, for multiple safflower filaments localization problems, the filament-necking localization method in this study can be combined with the connected region. By calculating the number of filaments in multiple connected regions and locating each of them in turn, the segmentation effect is shown in Fig. 15. The localization of multiple safflower filaments is finally realized. Therefore, the

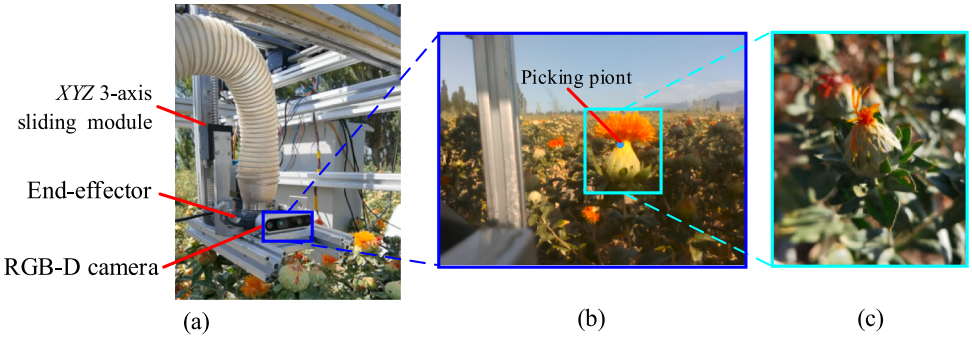

Fig. 14. Field experiments and results: (a) picking robot in field experiments; (b) results of camera localization for picking point; (c) results of filaments picking after localization.

Table 5
Data from the field test of safflower filament picking.

Weather conditions	Number of tests	Localization success rate/%	Breakage rate/%	Average running time/s
Sunny day with light	50	87.00	7.42	0.208
Sunny day with backlight	50	93.00	6.18	0.174
Overcast day with light	50	90.00	6.70	0.195
Cloudy day with light	50	85.00	7.96	0.233

Fig. 15. Segmentation results of multiple safflower filaments: (a)images of multiple filaments; (b) segmentation maps of the maximum connected region.

proposal can provide a reference for multiple subsequent studies on filament localization and quality picking.

7. Conclusions and future works

Influenced by complex environments of light intensity changes and crop shadows, the color and texture features of safflower became unclear. Safflower-picking robots had difficulty with safflower recognition and picking point localization. To solve the above difficulties in safflower identification and picking point localization, combining improved PSO with a rotated rectangle algorithm based on the filament-necking localization method for safflower-picking robots was proposed.

In the future, the primary segmentation and re-segmentation algorithms in the filament-necking localization method need to be further optimized. (i) The improved PSO algorithm handles the computational efficiency inefficiently during the primary segmentation. (ii) The circular ROI can be appropriately reduced to better fit the region of the picking point for different sizes of safflower filaments. In addition, the computational efficiency of the method should be improved if the method was applied for some tasks running in real time, such as disease localization spraying of safflower.

CRediT authorship contribution statement

Zhenyu Xing: Funding acquisition, Conceptualization, Methodology, Formal analysis, Writing – original draft, Visualization, Supervision. **Zhenguo Zhang:** Writing – review & editing, Data curation. **Ruimeng Shi:** Conceptualization, Methodology, Software, Writing – review & editing. **Quanfeng Guo:** Software, Formal analysis. **Chao Zeng:** Resources, Visualization.

Declaration of Competing Interest

The authors declare that they have no known competing financial interests or personal relationships that could have appeared to influence the work reported in this paper.

Data availability

The authors do not have permission to share data.

Acknowledgments

This work is supported in part by the National Natural Science Foundation of China under Grant 52265041 and 31901417, in part by Open Subjects of Zhejiang Provincial Key Laboratory for Agricultural Intelligent Equipment and Robotics, China under Grant 2022ZJZD2202, and in part by Graduate School-level Research and Innovation Program of Xinjiang Agricultural University, China under Grant XJAUGRI2023021. The authors also acknowledge the Key Laboratory of Xinjiang Intelligent Agricultural Equipment, China for their assistance in conducting field experiments, and the University of Adelaide, Australia for Dr. Yongliang Qiao in writing guidance.

References

Abbood, W.T., Abdullah, O.I., Khalid, E.A., 2020. A real-time automated sorting of robotic vision system based on the interactive design approach. Int. Jour. Int. Des. Manufact. 14, 201–209. https://doi.org/10.1007/s12008-019-00628-w.

Almoujahed, M.B., Rangarajan, A.K., Whetton, R.L., Vincke, D., Eylenbosch, D., Vermeulen, P., Mouazen, A.M., 2022. Detection of fusarium head blight in wheat under field conditions using a hyperspectral camera and machine learning. Comput. Electron. Agric. 203, 107456 https://doi.org/10.1016/j.compag.2022.107456.

Bai, Y., Zhang, B., Xu, N., Zhou, J., Shi, J.Y., Diao, Z.H., 2023. Vision-based navigation and guidance for agricultural autonomous vehicles and robots: A review. Comput. Electron. Agric. 205, 107584 https://doi.org/10.1016/j.compag.2022.107584.

Behroozi-Khazaei, N., Maleki, M.R., 2017. A robust algorithm based on color features for grape cluster segmentation. Comput. Electron. Agric. 142, 41–49. https://doi.org/10.1016/j.compag.2017.08.025.

Benbarrad, T., Salhaoui, M., Kenitar, S.B., Arioua, M., 2021. Intelligent machine vision model for defective product inspection based on machine learning. Jour. Sen. Act. Net. 10 (1), 7. https://doi.org/10.3390/jsan10010007.

Campos, Y., Sossa, H., Pajares, G., 2016. Spatio-temporal analysis for obstacle detection inagricultural videos. Appl. Soft. Comput. 45, 86–97. https://doi.org/10.1016/j.asoc.2016.03.016.

Castillo-Martínez, M.Á., Gallegos-Funes, F.J., Carvajal-Gámez, B.E., Sosaa, G.U., Rosales-Silva, A.J., 2020. Color index based thresholding method for background and

foreground segmentation of plant images. Comput. Electron. Agric. 178, 105783 https://doi.org/10.1016/j.compag.2020.105783.
Chen, F., Ge, Y., Zhang, L.X., Qi, Z.H., Zeng, H.H., 2021. Design and experiment of the strip-collected pre-positioning mechanism for safflower picking robots. Trans. Chinese Soc. Agric. Eng. 37 (15), 10–19. https://doi.org/10.11975/j.issn.1002-6819.2021.15.002.
Chithra, P.L., Henila, M., 2021. Apple fruit sorting using novel thresholding and area calculation algorithms. Soft. Comput. 25 (1), 431–445. https://doi.org/10.1007/s00500-020-05158-2.
De Oliveira Neto, S.S., Zeffa, D.M., Freiria, G.H., Zoz, T., da Silva, C.J., Zanotto, M.D., Sobrinho, R.L., Alamri, S.A., Okla, M.K., AbdElgawad, H., 2022. Adaptability and Stability of Safflower Genotypes for Oil Production. Plants. 11, 708. https://doi.org/10.3390/plants11050708.
Dischinger, L.M., Cravetz, M., Dawes, J., Votzke, C., VanAtter, C., Johnston, M.L., Grimm, C.M., Davidson, J.R., 2021. Towards intelligent fruit picking with in-hand sensing[C]//2021. In: IEEE/RSJ International Conference on Intelligent Robots and Systems (IROS), pp. 3285–3291. https://doi.org/10.1109/IROS51168.2021.9636341.
Fan, P., Lang, G.D., Yan, B., Lei, X.Y., Guo, P.J., Liu, Z.J., Yang, F.Z., 2021. A method of segmenting apples based on gray-centered RGB color space. Remote. Sens. 13 (6), 1211. https://doi.org/10.3390/rs13061211.
Gao, G.M., Guo, H., Zhou, W., Luo, D., Zhang, J., 2023. Design of a control system for a safflower picking robot and research on multisensor fusion positioning. Engenharia. Agrícola. 43, e20210238.
Gao, L., Lin, X., 2018. A method for accurately segmenting images of medicinal plant leaves with complex backgrounds. Comput. Electron. Agric. 155, 426–445. https://doi.org/10.1016/j.compag.2018.10.020.
Ge, Y., Zhang, L.X., Gu, J.W., Fu, W., Zhu, R.G., Zhang, H.M., 2015. Parameter optimization and experiment of dual roller harvesting device for safflower. Trans. Chinese Soc. Agric. Eng. 2015, 31(21): 35-42. 10.11975/j.issn.1002-6819.2015.21.005.
Gongal, A., Amatya, S., Karkee, M., Zhang, Q., Lewis, K., 2015a. Sensors and systems for fruit detection and localization: A review. Comput. Electron. Agric. 116, 8–19. https://doi.org/10.1016/j.compag.2015.05.021.
Gongal, A., Silwal, A., Amatya, S., Karkee, M., Zhang, Q., Lewis, K., 2015b. Apple crop-load estimation with over-the-row machine vision system. Comput. Electron. Agric. 120, 26–35. https://doi.org/10.1016/j.compag.2015.10.022.
Gongora, B., de Souza, S.N., M., Bassegio, D., Santos, R.F., Siqueira JA, C., Bariccatti, R. A., Gurgacz, F., Secco, D., Tokura, L.K., Sequinel, R.,, 2022. Comparison of emissions and engine performance of safflower and commercial biodiesels. Ind. Crops. Prod. 179, 114680 https://doi.org/10.1016/j.indcrop.2022.114680.
Granland, K., Newbury, R., Chen, Z., Ting, D., Chen, C., 2022. Detecting occluded Y-shaped fruit tree segments using automated iterative training with minimal labeling effort. Comput. Electron. Agric. 194, 106747 https://doi.org/10.1016/j.compag.2022.106747.
Janković, J., 2022. Projektovanje sistema za skeletizaciju slika zasnovanog na Zhang-Suen algoritmu. In: 2022 30th Telecommunications Forum (TELFOR). IEEE, pp. 1–4. https://doi.org/10.1109/TELFOR56187.2022.9983743.
Jatmiko, W., Sekiyama, K., Fukuda, T., 2007. A pso-based mobile robot for odor source localization in dynamic advection-diffusion with obstacles environment: theory, simulation and measurement. IEEE Computational Intelligence Magazine. 2 (2), 37–51. https://doi.org/10.1109/MCI.2007.353419.
Jiang, H., Sun, X., Fang, W., Fu, L.S., Li, R., Cheein, F.A., Majeed, Y., 2023. Thin wire segmentation and reconstruction based on a novel image overlap-partitioning and stitching algorithm in apple fruiting wall architecture for robotic picking. Comput. Electron. Agric. 209, 107840 https://doi.org/10.1016/j.compag.2023.107840.
Kumar, A., Kumar, A., Vishwakarma, A., Singh, G.K., 2022. Multilevel thresholding for crop image segmentation based on recursive minimum cross entropy using a swarm-based technique. Comput. Electron. Agric. 203, 107488 https://doi.org/10.1016/j.compag.2022.107488.
Leborgne, A., Mille, J., Tougne, L., 2015. Noise-resistant digital euclidean connected skeleton for graph-based shape matching. Jour. Visual. Communic. Image. Represent. 31, 165–176. https://doi.org/10.1016/j.jvcir.2015.06.005.
Li, K., Gong, W.X., Shi, Y.G., Li, L., He, Z., Ding, X.T., Wang, Y.C., Ma, L., Hao, W., Yang, Z., Cui, Y.J., 2023a. Predicting positions and orientations of individual kiwifruit flowers and clusters in natural environments. Comput. Electron. Agric. 211, 108039 https://doi.org/10.1016/j.compag.2023.108039.
Li, B.R., Long, Y., Song, H.B., 2018. Detection of green apples in natural scenes based on saliency theory and Gaussian curve fitting. Int. J. Agric. Biol. Eng. 11 (1), 192–198. https://doi.org/10.25165/j.ijabe.20181101.2899.
Li, J., Qiao, Y., Liu, S., Zhang, J., Yang, Z., Wang, M., 2022. An improved YOLOv5-based vegetable disease detection method. Comput. Electron. Agric. 202, 107345. https://doi.org/10.1016/j.compag.2022.107345.
Li, D.H., Shen, M.M., Li, D., Yu, X., 2017. Green apple recognition method based on the combination of texture and shape features. In: In: 2017 International Conference on Mechatronics and Automation (ICMA). IEEE, pp. 264–269. https://doi.org/10.1109/ICMA.2017.8015825.
Li, T., Xie, F., Zhao, Z., Zhao, H., Guo, X., Feng, Q.C., 2023b. A multi-arm robot system for efficient apple harvesting: Perception, task plan and control. Comput. Electron. Agric. 211, 107979 https://doi.org/10.1016/j.compag.2023.107979.
Liu, X., Zhao, D., Jia, W., Tang, S.P., Shen, T., 2016. A method of segmenting apples at night based on color and position information. Comput. Electron. Agric. 122, 118–123. https://doi.org/10.1016/j.compag.2016.01.023.
Luo, L.F., Zou, X.J., Xiong, J.T., Zhang, Y., Peng, H.X., Lin, G.C., 2015. Automatic positioning for picking point of grape picking robot in natural environment. Trans. Chinese Soc. Agric. Eng. 31 (2), 14–21. https://doi.org/10.3969/j.issn.1002-6819.2015.02.003.
Montoya-Cavero, L.E., León, T.R.D., Gómez-Espinosa, A., Cabello, J.A.E., 2022. Vision systems for harvesting robots: Produce detection and localization. Comput. Electron. Agric. 192, 106562 https://doi.org/10.1016/j.compag.2021.106562.
Pandey, S., Wu, L., Guru, S. M., Buyya, R., 2010. A particle swarm optimization-based heuristic for scheduling workflow applications in cloud computing environments. In 2010 24th IEEE international conference on advanced information networking and applications (pp. 400-407). IEEE, 400-407. 10.1109/AINA.2010.31.
Qiao, Y., Guo, Y., He, D., 2023. Cattle body detection based on YOLOv5-ASFF for precision livestock farming. Comput. Electron. Agric. 204, 107579. https://doi.org/10.1016/j.compag.2022.107579.
Qiao, Y., Truman, M., Sukkarieh, S., 2019. Cattle segmentation and contour extraction based on Mask R-CNN for precision livestock farming. Comput. Electron. Agric. 165, 104958 https://doi.org/10.1016/j.compag.2019.104958.
Rico-Fernández, M.P., Rios-Cabrera, R., Castelán, M., Guerrero-Reyes, H.I., Juarez-Maldonado, A., 2019. A contextualized approach for segmentation of foliage in different crop species. Comput. Electron. Agric. 156, 378–386. https://doi.org/10.1016/j.compag.2018.11.033.
Ritu, G., Kumar, S.A., 2014. Multi-objective workflow grid scheduling using ε-fuzzy dominance sort based discrete particle swarm optimization. J. Supercomput. 68 (2), 709–732. https://doi.org/10.1007/s11227-013-1059-8.
Rong, Q., Hu, C., Hu, X., Xu, M., 2023. Picking point recognition for ripe tomatoes using semantic segmentation and morphological processing. Comput. Electron. Agric. 210, 107923 https://doi.org/10.1016/j.compag.2023.10792.
Sabzi, S., Abbaspour-Gilandeh, Y., Hernandez-Hernansez, J.L., Azadshahraki, F., Karimzadeh, R., 2019. The use of the combination of texture, color and intensity transformation features for segmentation in the outdoors with emphasis on video processing. Agric. 9 (5), 104. https://doi.org/10.3390/agriculture9050104.
Singh, S., Mittal, N., Thakur, D., Singh, H., Oliva, D., Demin, A., 2021a. Nature and biologically inspired image segmentation techniques. Comput. Electron. Agric. 2021a, 1–28. https://doi.org/10.1007/s11831-021-09619-1.
Singh, N., Tewari, V.K., Biswas, P.K., Pareek, C.M., Dhruw, L.K., 2021b. Image processing algorithms for in-field cotton boll detection in natural lighting conditions. Artif. Intell. Agric. 5, 142–156. https://doi.org/10.1016/j.aiia.2021.07.002.
Soltani, F.M., Sardari, H., 2022. Defect detection in fruit and vegetables by using machine vision systems and image processing. Food. Eng. Reviews. 14 (3), 353–379. https://doi.org/10.1007/s12393-022-09307-1.
Su, D.B.L.G., Qiao, Y.L., Kong, H., Sukkarieh, S., 2021. Real time detection of inter-row ryegrass in wheat farms using deep learning. Biol. Eng. 204, 198–211. https://doi.org/10.1016/j.biosystemseng.2021.01.019.
Tian, Z., Zhang, B.W., Chen, H., Shen, C.H., 2022. Instance and panoptic segmentation using conditional convolutions. IEEE Transactions on Pattern Analysis and Machine Intelligence 45 (1), 669–680. https://doi.org/10.1109/TPAMI.2022.3145407.
Ulzii-Orshikh, D., Malrey, L., Sang-seok, Y., 2017. An yield estimation in citrus orchards via fruit detection and counting using image processing. Comput. Electron. Agric. 140, 103–112. https://doi.org/10.1016/j.compag.2017.05.019.
Wang, Y., Gu, L.J., Jiang, T., Gao, F., 2023. MDE-UNet: A Multitask Deformable UNet Combined Enhancement Network for Farmland Boundary Segmentation. IEEE Geoscience and Remote Sensing Letters 20, 1–5. https://doi.org/10.1109/LGRS.2023.3252048.
Wang, D.D., He, D.J., Song, H.B., Liu, C., Xiong, H.T., 2019b. Combining SUN-based visual attention model and saliency contour detection algorithm for apple image segmentation. Multimed. Tools Appl. 78 (13), 17391–17411. https://doi.org/10.1007/s11042-018-7106-y.
Wang, J.H., Lin, Y.Z., Liu, R.R., Fu, J., 2022. Odor source localization of multi-robots with swarm intelligence algorithms: A review. Front. Neur. 16, 949888 https://doi.org/10.3389/fnbot.2022.949888.
Wang, C.L., Lu, C.Y., Chen, W.Z., Li, H.W., He, J., Wang, Q.J., 2019a. Image segmentation of maize stubble row based on genetic algorithm and threshold filtering noise. Trans. Chinese Soc. Agric. Eng. 35 (16), 198–205. https://doi.org/10.11975/j.issn.1002-6819.2019.16.022.
Xiang, R., 2018. Image segmentation for whole tomato plant recognition at night. Comput. Electron. Agric. 154, 434–442. https://doi.org/10.1016/j.compag.2018.09.034.
Xiong, J.T., He, Z.L., Tang, L.Y., Lin, R., Liu, Z., 2017. Visual Localization of Disturbed Grape Picking Point in Non-structural Environment. Trans. Chinese Soc. Agric. Mach. 48(4), 29-33, 81. 10.6041/j.issn.1000-1298.2017.04.003.
Xue, X., Zhou, G.M., Qiu, Y., Li, Z., Wang, J., Hu, L., Fan, J.C., Guo, X.M., 2019. Detection of young green apples in orchard environment using adaptive ratio chromatic aberration and HOG-SVM. Computer and Computing Technologies in Agriculture: CCTA 2017: Computer and Computing Technologies in Agriculture XI pp. 253-268. 10.1007/978-3-030-06137-1_24.
Yogesh., Dubey, A.K., Ratan, R., Rocha, A.,, 2020. Computer vision based analysis and detection of defects in fruits causes due to nutrients deficiency. Cluster. Comput. 23, 1817–1826. https://doi.org/10.1007/s10586-019-03029-6.
Zhang, Z.G., Xing, Z.Y., Yang, S.P., Feng, N., Liang, R.Q., Zhao, M.Y., 2022. Design and experiments of the circular arc progressive type harvester for the safflower filaments. Trans. Chinese Soc. Agric. Eng. 38 (17), 10–21. https://doi.org/10.11975/j.issn.1002-6819.2022.17.002.
Zhang, Z.G., Shi, R.M., Xing, Z., Y.Guo, Q.F., Zeng, C., 2023a. Improved Faster Region-Based Convolutional Neural Networks (R-CNN) Model Based on Split Attention for the Detection of Safflower Filaments in Natural Environments. Agronomy 13 (10), 2596. https://doi.org/10.3390/agronomy13102596.
Zhang, Z.G., Xing, Z.Y., Zhao, M.Y., Yang, S.P., Guo, Q.F., Shi, R.M., Zeng, C., 2023b. Detecting safflower filaments using an improved YOLOv3 under complex

environments. Chinese Soc. Agric. Eng. 39 (3), 162–170. https://doi.org/10.11975/j.issn.1002-6819.202211204.

Zhang, T., Y., Zhang, L, X., Ge, Y., Wang, H., Liu, G, X., 2018. Study on two dimensional center point calibration method for safflower filaments. Comput. Eng. Appl. 54 (15), 176–180. https://doi.org/10.3778/j.issn.1002-8331.1801-0136.

Zhong, Z., Xiong, J.T., Zheng, Z.H., Liu, B.L., Liao, S.S., Huo, Z.W., Yang, Z.G., 2021. A method for litchi picking points calculation in natural environment based on main fruit bearing branch detection. Comput. Electron. Agric. 189, 106398 https://doi.org/10.1016/j.compag.2021.106398.

Zhou, T., Fu, H.Z., Gong, C., Shao, L., Porikli, F., Ling, H.B., Shen, J.B., 2022. Consistency and diversity induced human motion segmentation. IEEE Transactions on Pattern Analysis and Machine Intelligence 45 (1), 197–210. https://doi.org/10.1109/TPAMI.2022.3147841.

Zou, K., Ge, L., Zhou, H., Zhang, C., Li, W., 2022. An apple image segmentation method based on a color index obtained by a genetic algorithm. Multimed. Tools Appl. 81 (6), 8139–8153. https://doi.org/10.1007/s11042-022-11905-4.